

SonoPrint: Acoustically Assisted Volumetric 3D Printing for Composites

Prajwal Agrawal, Shengyang Zhuang, Simon Dreher, Sarthak Mitter, and Daniel Ahmed*

Advances in additive manufacturing in composites have transformed aerospace, medical devices, tissue engineering, and electronics. A key aspect of enhancing properties of 3D-printed objects involves fine-tuning the material by embedding and orienting reinforcement within the structure. Existing methods for orienting these reinforcements are limited by pattern types, alignment, and particle characteristics. Acoustics offers a versatile method to control the particles independent of their size, geometry, and charge, enabling intricate pattern formations. However, integrating acoustics into 3D printing has been challenging due to the scattering of the acoustic field between polymerized layers and unpolymerized resin, resulting in unwanted patterns. To address this challenge, SonoPrint, an innovative acoustically assisted volumetric 3D printer is developed that enables simultaneous reinforcement patterning and printing of the entire structure. SonoPrint generates mechanically tunable composite geometries by embedding reinforcement particles, such as microscopic glass, metal, and polystyrene, within the fabricated structure. This printer employs a standing wave field to create targeted particle motifs—including parallel lines, radial lines, circles, rhombuses, hexagons, and polygons—directly in the photosensitive resin, completing the print in just a few minutes. SonoPrint enhances structural properties and promises to advance volumetric printing, unlocking applications in tissue engineering, biohybrid robots, and composite fabrication.

as aerospace,^[1–3] automobiles,^[4] construction,^[5–7] medicine,^[8–14] and more. “Composite” refers to a structure constructed from two or more materials: a continuous phase, the matrix, and a discontinuous phase, the reinforcement, that adds strength to the structure.^[15] Alignment of the reinforcement in a composite can significantly improve the structure’s mechanical properties, that is (i.e.), its strength, stiffness, and toughness, by creating more efficient load transfer pathways and reducing stress concentrations between the matrix and reinforcement.^[16] Thus, composite structures offer improved performance.^[17,18] Current methods for aligned reinforcement involve passive or active forces.^[19–23] Active approaches that rely on external energy sources—such as electric, magnetic, or acoustic fields—to pattern microparticle motifs provide higher control and precision compared to methods that utilize shear,^[24–27] gravitational,^[28] hydrodynamic,^[29,30] and other such forces for alignment of microparticles.^[31–38] These approaches also promote more precise alignment and offer greater flexibility in the types and shapes of patterns created, enabling more robust particle


1. Introduction

Recent years have seen a growing interest in additive manufacturing of composite structures due to their high strength-to-weight ratio, corrosion resistance, and design flexibility, features which make composites attractive for industries such

alignment inside a manufactured geometry.^[33]

Although electric,^[19,39–45] and magnetic,^[20,46–51] field-assisted reinforcement strategies have been applied to 3D printing of composites, both depend on intrinsic properties of the particles, such as surface charge and magnetism, and are therefore limited in their choice of materials.^[19,21,46] In contrast, acoustics offers an alternative modality for manipulating microscopic particles within a host resin, as the effect of sound on particles is independent of features such as size, geometry, and charge.^[52–60] However, incorporating acoustics into conventional 3D printing methods, such as vat polymerization-based techniques^[23,61–64] presents a challenge in achieving consistent patterning in a 3D geometry. As each layer is printed, a complex scattered acoustic field arises between the polymerized hard layers and the unpolymerized resin just above or below it, making control over the internal patterning of microparticles in the subsequent layers challenging.^[23,61,62,64] Despite the applications and advantages offered by these methods, including ink diversity, particle connectivity, multimaterial printing, and others, these challenges still need to be addressed.^[23,61,62,64]

P. Agrawal, S. Zhuang, S. Dreher, S. Mitter, D. Ahmed
 Acoustic Robotics Systems Lab
 Institute of Robotics and Intelligent Systems
 Department of Mechanical and Process Engineering
 ETH Zurich
 Zurich, Switzerland
 E-mail: dahmed@ethz.ch

 The ORCID identification number(s) for the author(s) of this article can be found under <https://doi.org/10.1002/adma.202408374>

© 2024 The Author(s). Advanced Materials published by Wiley-VCH GmbH. This is an open access article under the terms of the [Creative Commons Attribution-NonCommercial](https://creativecommons.org/licenses/by-nc/4.0/) License, which permits use, distribution and reproduction in any medium, provided the original work is properly cited and is not used for commercial purposes.

DOI: [10.1002/adma.202408374](https://doi.org/10.1002/adma.202408374)

To address this challenge, the recently developed vat-polymerization-based manufacturing technology, known as volumetric printing, can be adapted, as it can maintain the acoustic pattern by printing structures as whole.^[65] Derived from the mathematical models of computed tomography (CT) and intensity modulated radiation therapy (IMRT) scans, this approach prints 3D structures as entire volumes, resulting in a faster build time compared to layer-by-layer additive manufacturing.^[65,66] To advance this technology with acoustic particle alignment, addressing the challenges of transmitting acoustic waves through high-viscosity resins (>10 Pa s) is crucial, as it presents difficulties for precise particle patterning.^[23,61,67] Conversely, using low-viscosity resins (<1 Pa s) leads to issues with particles settling too quickly after patterning in the vial. Therefore, a trade-off is necessary. To date, no acoustically-assisted volumetric printing techniques have been demonstrated.

Here, we introduce SonoPrint, an acoustically-assisted volumetric 3D printing technique that uses acoustic energy to trap and pattern microparticles within a volumetrically-fabricated 3D composite structure. In developing this technique, we constructed volumetric- and acoustic-compatible experimental setups featuring piezoelectric transducers (PZTs), index-matching liquid, and a vial filled with resin (matrix) and microparticles (reinforcement). The reinforcement consisted of various materials such as glass, polystyrene, metal, and in sizes from 1 to 250 micrometer—were embedded in di-pentaerythritol pentaacrylate resin (PETA). Using various numbers of PZTs in different configurations and frequencies, we achieved patterning in the form of parallel lines, radial lines, circles, rhombuses, quadrilaterals, hexagons, and polygons. The size, thickness, and spacing of pattern units were controllable based on the PZT configurations; for example, we produced lines separated by 0.46–0.96 mm. Through volumetric printing, we successfully incorporated these patterned microparticles into composite geometries within minutes. Optimization of the parameters yielded composite structures with a sub-millimeter feature size. Mechanical tests, including tensile and compression tests, showed increases in strength of $\approx 46\%$ and 13% , respectively, for structures with aligned versus randomly distributed microparticles.

2. Results and Discussion

2.1. Experimental Setup

SonoPrint comprises several components, including a projector, a glass vial (hereafter termed vial), a rotation mechanism, an acoustic setup, a function generator, an amplifier, a control unit, and a software. The projector casts images generated by the software onto a rotating vial containing photosensitive liquid resin and microparticles, as shown in **Figure 1A**. The vial is immersed in an index-matching liquid. The acoustic setup consists of PZTs arranged around the vial, which are controlled by a function generator and an amplifier to generate an acoustic wavefield. The resonance frequencies of the PZTs were verified using an oscilloscope. **Figure 1A,B** depicts the SonoPrint system components alongside a model geometry being fabricated.

When patterning microparticles within the vial, we utilized three acoustic setups, each equipped with two, four, and six PZTs,

respectively. The two- and four- PZT setups were made compatible with volumetric printing by incorporating light transmission through front and back transparent glass panels. PZTs on the remaining sides produced bulk acoustic waves. Each setup comprised a transparent glass vial with a refractive index (RI) of 1.516, surrounded by glycerol as index matching liquid with an RI of 1.4731.^[68] Glycerol had negligible impact on acoustic transmission, with acoustic attenuation loss of 0.5%. Also, it has a better refractive index matching with the resins and the glass vial. The PZTs were connected to a function generator and amplifier to generate a standing acoustic wavefield in the vial to align and pattern microparticles, see **Figure 1C**. We also studied the acoustic energy efficiency, which resulted in $\approx 14\%$ at the center of the vial (see **Text S1** and **Figures S1** and **S2**, Supporting Information). In the six-PZT setup, where no light can pass through due to PZTs covering all six sides (see **Figure 2A**), the vial—once the desired microparticle pattern is achieved—is transferred to a square container made of glass on all four sides to facilitate volumetric printing, see **Figure S8** in the Supporting Information.

In our study of microparticle patterning, we tested various microparticles, including polystyrene ($\approx 15\ \mu\text{m}$), soda-lime glass (≈ 22), and stainless steel (≈ 11) (see Methods for specific size range of microparticles). When exposed to a standing acoustic wavefield, the microparticles were subjected to acoustic radiation forces.^[53,67,69–72] To determine the directionality of the force, we calculated the acoustic contrast factor Φ , which is positive for all tested particle types, indicating movement towards the pressure nodal position.^[67,73] We further investigated the acoustic parameters, such as frequency and amplitude, to achieve desired microparticle patterns, see **Movie S1** (Supporting Information) for a line pattern using 1 MHz PZTs and **Movie S2** (Supporting Information) for quadrilateral pattern. Finally, we evaluated the compatibility of the SonoPrint printer system with PETA (0.28–11.8 Pa s; see **Figure S11** in the Supporting Information).

After achieving the desired acoustic patterning, as shown in **Figure 1C**, we turned off the PZTs and proceeded with volumetric printing to create structures containing the patterned microparticles. In this process, the desired 3D model in standard triangle language (STL) is uploaded in the volumetric printing software, which generates a series of 2D images.^[65,74,75] Typically, one image is generated for each rotation angle, resulting in 360 images for a complete 360-degree rotation.^[65] These images are then projected onto the vial's center, which holds the polymerizable resin and patterned microparticles. During this phase, the vial is rotated to ensure each image is projected at the correct angle; as illustrated in **Figure 1B**. Polymerization is initiated upon reaching a significant energy threshold by the projected light (also see **Figure S12** in the Supporting Information), which usually takes 30–240 s resulting in the formation of 3D structures, as shown in **Figure 1D** and **Movie S3** in the Supporting Information. After fabrication, the structures were removed from the vial, and cleaned (see the Experimental Section). We examined the pattern formations in the fabricated geometries. Finally, we assessed the feature size of the printed geometries using scanning electron microscopy (SEM) (see **Figure S17**, Supporting Information) and mechanical strength of the structures using tensile and compression tests.

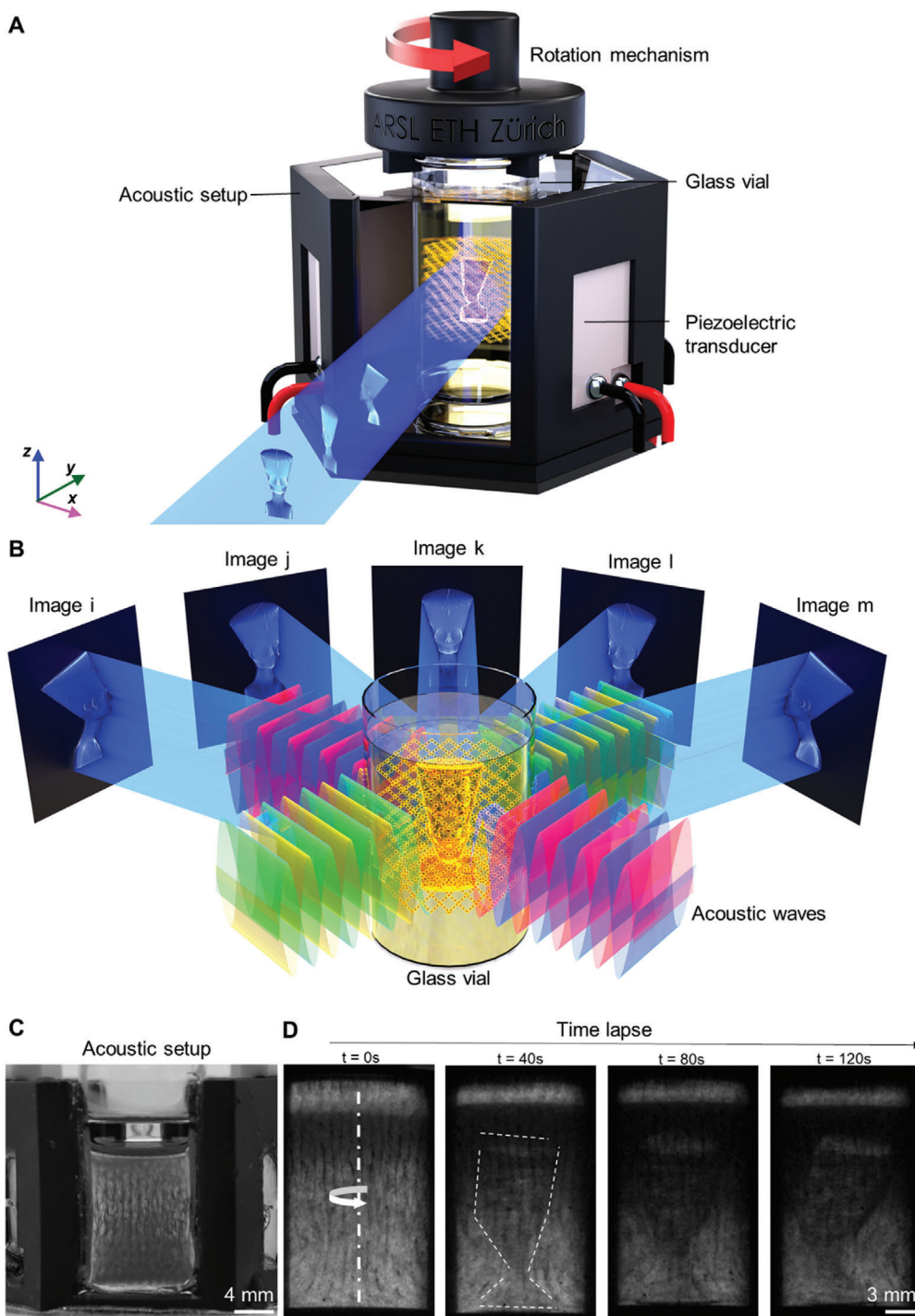


Figure 1. SonoPrint: An acoustically assisted volumetric 3D printer. A) Schematic illustrating the setup of a SonoPrint printer. Images of Nefertiti bust model geometry are being projected on a rotating glass vial (hereafter termed as vial) focused at the center of the vial. The vial contains photopolymerizable resin with acoustically aligned microparticles. A four piezoelectric transducer (PZT)–setup is used for the patterning of microparticles. A Nefertiti bust model geometry is also formed within the vial surrounded by index-matching liquid. B) The schematic illustrates the generation of bulk acoustic waves by the PZTs and their transmission through the vial to pattern the microparticles inside the resin. Image projections from i to m illustrate the projections of various images generated by volumetric software that are projected at different angles and at their corresponding times. As shown in the schematics, this results in the fabrication of a composite model geometry of Nefertiti bust with patterned microparticles in a desired manner. C) Images show side view of 1–22 micrometer stainless-steel microspheres patterned in di-pentaerythritol pentaacrylate resin (PETA) in the four–PZT acoustic setup, with all four PZTs excited at 1.01 MHz and 30 V_{pp}, with the temperature maintained at 25 °C. Scale bar: 4 mm. D) This figure illustrates the fabrication of 3D Nefertiti bust composite geometry over a time span of 120 s with microparticle pattern obtained in (C), also see Movie S3 in the Supporting Information.

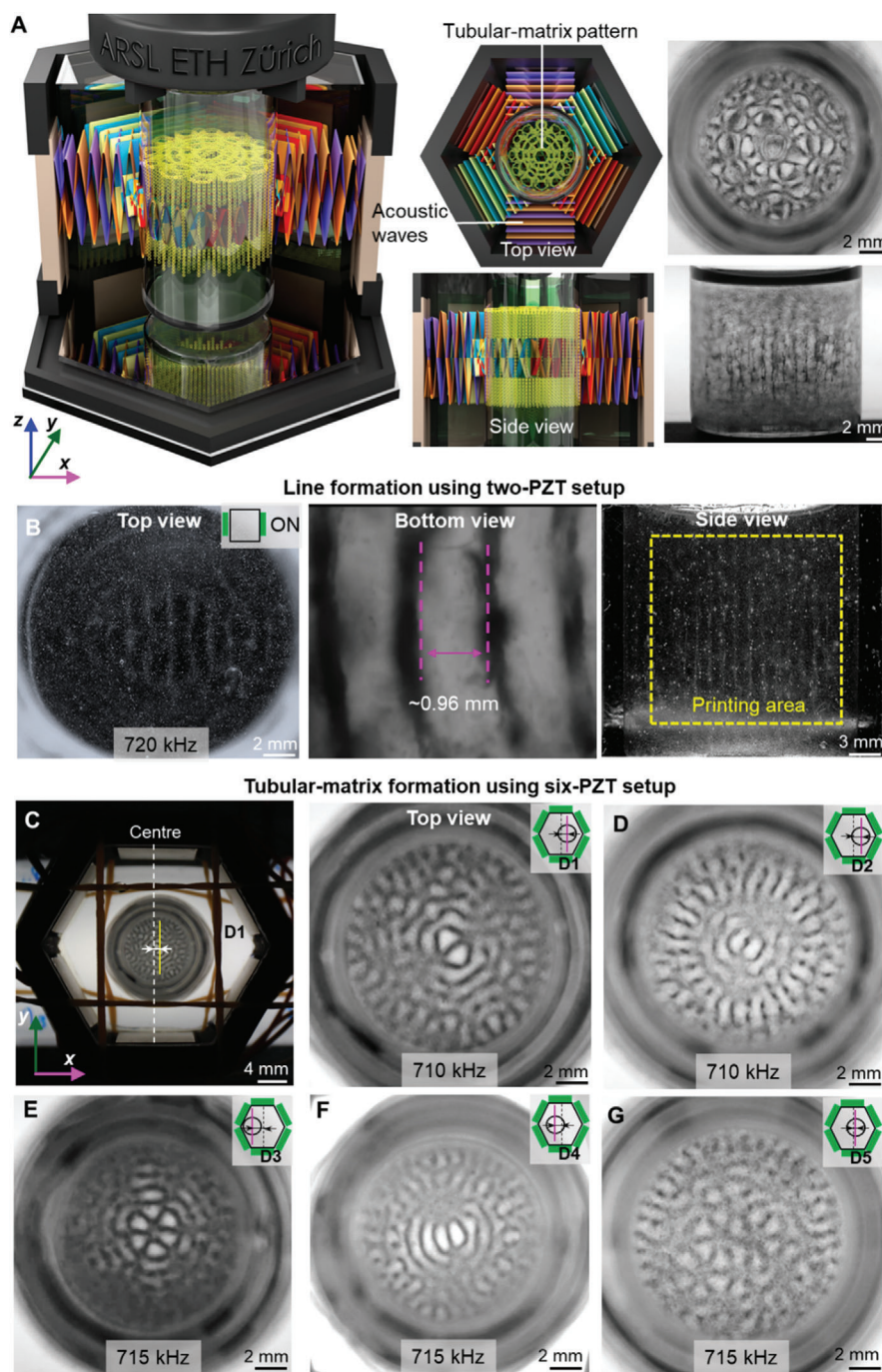


Figure 2. Acoustic patterning of microparticles. A) A schematic representation of a six piezoelectric transducer (PZT)– acoustic setup that utilizes six identical PZTs orthogonally positioned in xz -plane being actuated simultaneously at resonance frequency to produce bulk acoustic waves for patterning microparticles in the desired manner. A top and side view of the setup also illustrates the patterns from these views. Displays the top and side view of the six– PZT setup when the glass vial (hereafter termed vial) is placed at the center on the glass plate of the acoustic setup and all six PZT are actuated in the 715 kHz setup, using stainless steel microspheres in di-pentaerythritol pentaacrylate resin (PETA). It shows the patterns as generated in illustration in (A). The vial was placed at the center of the acoustic setup with standard deviation of ± 1.5 mm. In all experiments PZTs were excited at $30 V_{pp}$ and temperature was maintained between $25\text{--}30$ °C. B) Shows images of 1.02 MHz two– PZT acoustic setup’s top, bottom-microscopic, and side views. Glass microspheres were used in PETA. C) Illustrates the 710 kHz six– PZT acoustic setup. The zoomed in view shows the vial located at D1, i.e., $\approx 0.7 \pm 0.4$ mm distance from the center of the acoustic setup. Stainless steel microspheres were used. D) Image shows microparticle pattern generated in the 710 kHz six– PZT setup by moving the vial along the x -axis by D2, i.e., $\approx 0.9 \pm 0.5$ mm from the extreme corner of the acoustic setup. Stainless steel microspheres were used. E–G) A top view of the patterning is shown in relation to the change in placement of the vial container relative to the x -axis following excitation of all six PZTs in the 715 kHz six– PZT acoustic setup. Patterns were formed with stainless steel microspheres. The vial was moved along x -axis at distance D3–D5, corresponds to $\approx -3.3 \pm 0.4$ mm, $\approx -1.1 \pm 0.7$ mm, and $\approx 0.5 \text{ mm} \pm 1.2$ mm distances from the center of the setup.

2.2. Acoustic Patterning of Microparticles and Pattern Characterization

We began the acoustic patterning experiments by using a two-PZT acoustic setup to create planar sheet patterns, then advanced to more intricate configurations using a four- and six- PZT setup. In the two- PZT configuration, a pair of parallel PZTs was placed opposite each other and with simultaneous acoustic excitation at the same frequency and voltage, they generated a standing acoustic wavefield within the vial, as shown in Figure S5A in the Supporting Information. This wavefield consisted of a series of pressure nodes and antinodes, in which acoustic forces pushed the micron glass microspheres toward the pressure nodes, resulting in microparticle patterns in the x -direction and distributed as sheets in the yz -plane. To vary the spacing between the formed sheet patterns, we used PZTs of different resonant frequencies. For example, to adjust the spacing from 0.45 to 0.96 mm we used PZTs with resonance frequencies of 1.51, 1.02, and 720 kHz. The observed distance between two sheet plane varies by 5–20% compared to the theoretical calculations. Discrepancies between the calculated and practical distance values were observed, which can be attributed to the absence of information on the speed of sound for PETA resin at different temperatures. Initially, a two- PZT setup excited at 1.51 MHz, 30 V_{pp} and 25 °C with glass microspheres in PETA led to the formation of 2D plane patterns with a spacing of ≈ 0.45 mm, see Figure S5C in the Supporting Information. At 1.02 MHz, we achieved a distance of ≈ 0.68 mm between two planes, as depicted in Figure S5B in the Supporting Information. Similarly, employing a two-PZT setup at 720 kHz, we observed the formation of plane patterns with a separation distance of ≈ 0.96 mm from side, top, and bottom perspectives, as shown in Figure 2B. To maintain patterning consistency, in all experiments mentioned above and hereafter the excitation voltage was held constant at 30 volts, and the temperature was maintained between 25 and 30 °C by controlling the duration of ultrasound excitation. All patterns obtained in two- PZT setups can be reproduced in four- and six- PZT setups by exciting any pair of parallel PZTs.

Next, we studied the acoustic pattern in the four-PZT acoustic setup. The acoustic setup housed a hexagonal chassis, which incorporated four orthogonally positioned PZTs and two glass slides for light transmission. By activating these PZTs at 1.01 MHz produces quadrilateral patterns, (see Figure S7, Supporting Information) in the xy -plane, which were projected overall on the z -axis. We demonstrate the formation of rhombus patterns using 15 micrometer polystyrene particles by activating the PZT transducers at 1.01 MHz, as seen in Figure S7C, and Movie S2 in the Supporting Information. Additionally, stimulating a pair of parallel PZTs as in two- PZT setup resulted in sheet plane, see Movie S2 in the Supporting Information.

Finally, we investigated the acoustic pattern in a six-PZT acoustic setup arranged in a hexagonal configuration. We achieved a tubular-matrix pattern of stainless-steel microspheres by activating all six PZTs simultaneously at the same frequency, as shown in Figure 2A. This pattern was formed by positioning the vial in approximately center ± 1.5 mm using 715 kHz setup. We also observed dynamic pattern formation through straightforward manipulations of the vial within the acoustic chamber, which generated an infinite array of complex patterns. To fine-tune these

patterns, we adjusted the position of the vial along the x -axis while maintaining its center along the y -axis and the excitation frequency constant at 710–720 kHz. This approach led to a variety of tubular-matrix patterns. Figure 2C illustrates the six- PZT setup from a top view, showing the vial placed on the glass plate of the acoustic setup. To generate these tubular-matrix patterns, we began with the vial at position D1, i.e., ≈ 0.7 mm \pm 0.3 mm distance from the center of the acoustic setup. A second pattern, as shown in Figure 2D, was obtained by moving the vial along the x -axis to ≈ 0.9 mm \pm 0.5 mm from the center, as denoted by D2. Finally, we positioned the vial at three different positions, D3–D5, corresponding to ≈ -3.3 mm \pm 0.8 mm, ≈ -1.1 mm \pm 0.7 mm, and ≈ 0.5 mm \pm 1.2 mm distances from the center, respectively to obtain tubular patterns as shown in Figure 2E,G. These findings demonstrate that with our setups, multiple pattern types can be developed, and versatile, dynamic modulation of patterns is feasible in a controlled manner.

When patterning planes or 2D sheets, the resin temperature needs to be maintained between 20 and 30 °C. As the temperature increases, the resin viscosity decreases (see Text S1.4 and Figure S11, Supporting Information), making acoustic pattern feasible; however, at higher temperatures, the microparticles tend to settle faster due to gravity because of the lower viscosity of the resin, which can adversely affect the printing, see Figures S3 and S4 in the Supporting Information. For example, when the resin temperature is at 40 °C, the patterned stainless-steel microspheres in PETA sink and sheet pattern formation collapses within a few minutes. In addition, when PZTs are operated continuously at a high voltage for an extended period of time (a few minutes), the pattern formation also collapses due to the viscosity effects on temperature. For example, when PZTs were operated at 60 V_{pp} for 2 min, the resin temperature can rise from 25 °C to as high as 50 °C in PETA. To achieve stable pattern formation, the resin's viscosity needs to be maintained between 4 and 12 Pa s, i.e., corresponding to a temperature between 15 and 30 °C for a few minutes, sufficient for the printing process, which can be achieved by exciting the PZTs at low voltages or using pulsed excitations. In addition, the current acoustic setups in SonoPrint are limited to patterning microparticles up to 40 mm due to the height of the PZTs and particle settling in larger configurations.

2.3. Volumetric Printing

After achieving the desired pattern, the acoustic wavefield was turned off to initiate the polymerization process. For volumetric printing, we used a six- PZT setup. Once the pattern was established, the vial containing aligned microparticles was placed into the volumetric printing setup, shown in Figure S8 in the Supporting Information. Subsequently, to assess the consistency of microparticle patterning within 3D printed structures, we printed a cylindrical geometry and observed the patterns at various depth planes. The results showed that the distance between two planes had a patterning consistency of 91.27% over the printed structure, as shown in Text S3, and Figure S15A–D in the Supporting Information. To demonstrate straight and radial line pattern formation, we printed two Nefertiti bust structures—a benchmark against standard geometries—using stainless steel microspheres in PETA. We achieved the desired parallel and radial line patterns

consistently in the whole Nefertiti bust geometry by patterning them as defined in Figure 2, Figures S6 and S10 in the Supporting Information. The fabricated geometry and microparticle pattern are shown in Figure 3A,B, respectively. Additionally, a cylindrical structure with quadrilateral patterns of stainless-steel microspheres was printed, as shown in Figure 3C. This patterning was achieved by activating two pairs of parallel PZTs at 1.02 MHz.

To demonstrate complex printing with a variety of patterns, we reproduced miniaturized models of liver, heart, and lungs, with line, hexagonal, and polygon patterns respectively. By stimulating all six PZTs simultaneously at 710 kHz, the microparticles were patterned in hexagonal shapes. The printed liver geometry is shown in Figure 3D, and the resulted hexagonal pattern is shown in the zoomed-in view. A miniaturized hollow heart model was printed with line patterns by stimulating a pair of parallel PZTs at 715 kHz. Here, glass microspheres were patterned in rhodamine-mixed PETA. An image of the fabricated heart geometry is shown in Figure 3E. The zoomed-in figure illustrates the line pattern. Lastly, a model of the lungs was printed using stainless steel microspheres in three parts and then assembled together. In the first step, a polygonal tubular microparticle pattern was used in the left and right lungs as seen in Figure 2C. Alternatively, trachea was printed with horizontal line pattern, with two parallel PZTs excited at 715 kHz. Following this, the geometry was assembled together as shown in Figure 3F. The zoomed-in image shows microparticle patterning in the lungs and trachea.

2.4. Characterization, Analysis, and Applications of Printed Composite Geometry

We conducted mechanical tests to assess the mechanical strength of SonoPrint-fabricated structures in three configurations: (i) without microparticles, (ii) with randomly distributed particles, and (iii) with vertically aligned microparticles. The test samples were fabricated using PETA, incorporating stainless steel microspheres—20 mg of microparticles per 4 grams of PETA (also see Figures S13 and S14 in the Supporting Information). For both compression and tensile tests, the microparticles were aligned vertically, parallel to the direction of the applied force. To characterize the tensile test, we printed dog-bone-shaped structures with dimensions of 37.5 mm in height, 5.75 mm in width, and 2 mm in depth. For particle alignment, we utilized a two-PZT acoustic setup for patterning (see Figure 3G; Figure S16, Supporting Information), with one setup operating at 715 kHz and the other at 1.01 MHz.

The tensile strength of the acoustically aligned samples using the 1.01 MHz setup was measured to be $\approx 46\%$ higher than that of samples with randomly distributed microparticles (see Figure 3G). Next, we examined the mechanical behavior of the sample with respect to the number of sheet planes, which can be adjusted by the excitation acoustic frequency. We observed an $\approx 11\%$ change in tensile strength when increasing the number of microparticle-patterned sheet planes from 5 to 7 (715 kHz setup) to 8–10 (1.01 MHz setup), as shown in Figure 3G.

For the compression test, we printed cylindrical structures measuring 25.4 mm in height and 12.7 mm in diameter, see Figure 3H and Figure S17 in the Supporting Information. To align the microparticles vertically, we used a 1.51 MHz two-PZT

acoustic setup. The compression test revealed that specimens containing 24–28 sheet planes, which were acoustically aligned, exhibited $\approx 13\%$ increase in strength compared to samples with randomly distributed microparticles, as shown in Figure 3H. Our experiments demonstrate that the mechanical strength of the fabricated structures is enhanced by the alignment of microparticles.

3. Discussion

The SonoPrint system represents a novel advancement in volumetric 3D printing by incorporating acoustic assistance to align microparticles within various 3D structures. Our experimental results demonstrated the ability to print complex geometries, including the Nefertiti bust, Mario, and anatomical organs such as the heart, lungs, and liver, with aligned microparticles in diverse configurations such as parallel and radial lines, rhombuses, hexagons, and other polygons. We fabricated composite specimen using SonoPrint, which resulted in tensile and compression strengths increasing by $\approx 46\%$ and 13% , respectively, compared to structures with randomly distributed particles. Future work will investigate the mechanical properties of specimens embedding different shapes, directions, types, or sizes of microparticles.

We plan to explore the potential for generating selective patterns in different parts of the fabricated structure, which would allow further tuning of its mechanical properties. Currently, we are restricted to specific microparticle patterns. To enable diverse patterning within selective parts of the vial, a transducer array with multiple PZTs can be used. Additionally, the current SonoPrint setup incorporates 0.5 wt% of microparticles in the resin, which is relatively low compared to other printing methods such as extrusion.^[22,31,76–79] or vat-polymerization printing,^[23,61–64] techniques that can incorporate up to 10–15 wt% of microparticles.

SonoPrint can also contribute to developing new materials for biohybrid robots,^[80] and tissue constructs.^[81] This innovative approach holds potential for fabricating tissue constructs that mimic the physiology and functionality of specific biological tissues through complex cellular arrangements, which is critical for applications in tissue engineering and drug screening. For example, organizing cardiomyocytes into parallel lines is essential for the efficacy of cardiac constructs, while aligning endothelial cells is vital for creating functional vascular structures. Additionally, hexagonal patterns show promise for constructing liver tissue constructs. Volumetric printing has been demonstrated with various bioinks, including GelMA, hydrogels, silk-based bioinks, and others,^[82] suggesting that creating biohybrid and tissue constructs is feasible and highly effective.

4. Experimental Section

Volumetric Printer Hardware: The hardware for volumetric printer consists of a rotating vial made of glass (ETH Internal D-Phys Shop part number 40 053.1) onto which 2D image slices are projected, a light source (Si cube's SM9 with 405 nm wavelength), to generate the projection images, a lens to focus (Thorlabs, part number LA-1401A), a motor to control z-axis movement (Nema 17, Conrad order number: 1597325-AW), and an acoustic chamber which was fabricated using index-matching glass, self-cut into desired shape using glass slides (from Sigma Aldrich, part number: CLS294775×25) containing an index-matching liquid, i.e., glycerol (from

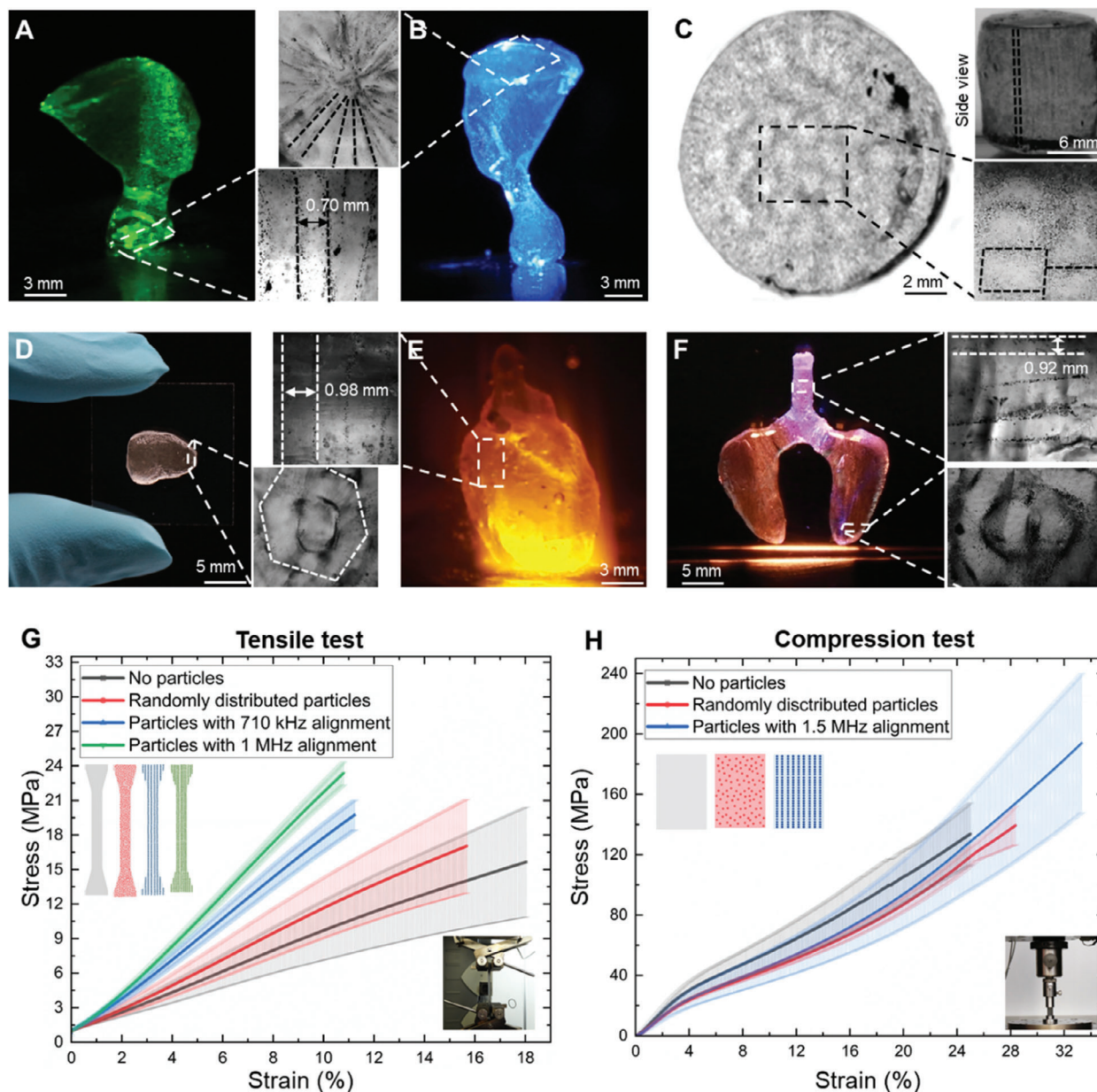


Figure 3. Analyses and characterization of the printed composite structures generated by the SonoPrint printer. A,B The image displays a complex Nefertiti bust composite geometry printed with parallel and radial line patterns respectively. Patterns in (A) were generated by actuating a pair of parallel piezoelectric transducer (PZT)s at 1.02 MHz and 25–30 °C, while the patterns in (B) were generated when the pair is actuated at 1.02 MHz, and 45–50 °C which was then rapidly cooled to achieve radial line pattern using stainless steel microspheres in di-pentaerythritol pentaacrylate resin (PETA). Also, a microscopic zoomed-in view shows the patterning. C) The images illustrate a cylindrical composite geometry with patterns generated by exciting two pair of parallel PZTs at 1.02 MHz with stainless steel microspheres mixed in PETA. The top, bottom and zoomed-in top view are shown. D) Displays a miniature printed liver geometry when held on a glass slide. An enlarged zoomed view illustrates the hexagonal patterning inside the geometry that was obtained by the excitation of all six PZTs at 710 kHz with stainless steel microspheres in PETA. E) The image shows a miniaturized hollow heart geometry with line patterning obtained by excitation of a pair of parallel PZTs at 715 kHz. The images are taken by shining a beam of blue light using a microscope. A zoomed in view shows the line pattern with glass microspheres in PETA. F) The figure depicts a miniaturized lung geometry, printed in three parts, where the right and left lungs have polygonal microparticle pattern, while the trachea incorporates horizontal lines. Six and two PZTs were excited at 710 kHz to achieve polygon and 715 kHz to achieve line pattern respectively with stainless steel microspheres in PETA. A zoomed-in view illustrates the pattern. G,H) The graph displays stress (MPa) versus strain (%) comparing results from tensile and compression tests respectively. The test samples were printed under three conditions: without microparticles, with randomly distributed microparticles, and with vertically aligned microparticles using sound waves in both tensile and compression tests. An image of the testing setup is shown in the bottom right corner. The sample patterning is visible in the middle left of the figure in 2D schematics. The graph data line represents the average of five samples tested for each condition across 400 points on the graph, error bar represents the standard deviations of the five samples at these points. The tensile test was performed using a two-PZT acoustic setup for patterning, with one setup using 715 kHz and the other 1.01 MHz. A 1.51 MHz two-PZT acoustic setup was used for the alignment of particles in compression tests. Error bars indicate the standard deviation for testing of five different samples.

Sigma Aldrich part number G5516-100ML) used for lesser light diffraction. The 2D slices generated by the software are projected at an intensity of $\approx 0.1\text{--}2.0\text{ mW cm}^{-2}$ at different angles but with consistent angular velocity onto the vial containing the photopolymerizable resin PETA, which is rotated via a stepper motor (Conrad part number: 1597325-AW). Volumetric curing of resin is depicted in Figure 1D and the fabricated 3D geometries are shown in Figure 3. The vial is confined in the acoustic chamber that generates the acoustic patterning initially. Local oxygen depletion is performed: an initial phase of free radical activation by light followed by rapid quenching, and then deactivation by oxygen. The acoustically patterned microparticles are also trapped inside the 3D geometry, making it a composite material with the patterned microparticles acting as reinforcement as shown in Figure 3.

Volumetric Printer Software: The software for the printer is based on the open-source code of Kelly et al.,^[65] which is modified to feature an easy-to-use graphical user interface (GUI), automation, and new parameters for scaling, optimizing the print and projection, and so on. The software is responsible for creating slices of a 3D object given in the form of a STL file and then projecting those slices onto the vial. First, the given STL file is voxelized with consideration of parameters such as the kinematics of the resin, projector specifications, and others.^[65] This is followed by optimizing and initializing the file using concepts of Radon and inverse Radon transform, biaxial thresholding, Fourier slice theorem, fast-Fourier transform, and more.^[65] The final step is the generation of a set of 2D images saved as mat files, which are then continuously looped through in the projection process.

Acoustic Hardware: The chassis used for the acoustic setup was designed in Solidworks and fabricated using Formlab Form 3+ and Ender 3 S1 3D printers. The glass slides (Sigma Aldrich part number: CLS294775x25) were reshaped using a glass cutter. Various frequency PZTs (Steminc, part numbers: SMPL20W15T14R111, SMPL20W15T21R111, and SMPL20W15T3R111) were first soldered to the connecting wires and then glued alongside the glass slides onto the fabricated chassis. The connections from the PZT were then connected to the function generator (Tektronics TTI AFG3011C) through an amplifier (Digitum electronics, part number: 85 184 030) to amplify the signal up to 60 V_{pp} at their resonance frequencies.

Overall Control Unit: The control of the setup was realized by the developed GUI. The projector was connected directly to a laptop/PC via an HDMI cable. An Arduino Mega 2560 with a CNC motor shield and A4988 motor drivers (Conrad, respective part numbers: 191790-AW, 1646889-AW, 1646889-AW) was controlling the motors, and it was also connected to the laptop/PC. Furthermore, the function generator and amplifier were either controlled through the GUI or manually for the frequency and amplitude optimization.

Resin Composition and Preparation: Di-pentaerythritol pentaacrylate was formulated with $0.6 \times 10^{-3}\text{ m}$ phenylbis (2,4,6 -trimethylbenzoyl) (Sigma Aldrich respective product numbers: 407 283 and 511 447). To achieve homogeneous mixing, they were heated to $100\text{ }^\circ\text{C}$ and simultaneously magnetically stirred at 500 rpm for up to an hour.^[65,83]

Microparticles Incorporation and its Mixing: The initial experiments used 5–50 micrometer glass beads (Cospheric part number: SLGMS-2.5 5–50 μm – 10 g), 15-micrometer polystyrene beads (Polysciences Polybead microspheres 15 μm catalogue number 18328-5), and 1–22 micrometer stainless steel microspheres (Cospheric part number: SSMMMS-7.8 1–22 μm – 10 g). Homogeneous mixtures were created by using magnetic stirrers at $80\text{ }^\circ\text{C}$ and 500 rpm to distribute particles with different concentrations of 5–120 mg of microparticles in 4 g of resin in order to achieve patterns of variable thicknesses in the resin, also see Figures S12–S14 in the Supporting Information. Before patterning, the resin was centrifuged for 15 s at 500 rpm and kept still for up to 10 min in order to eliminate bubbles and lower the resin temperature. Subsequently, resin with microparticles in the vial was placed in the acoustic setup under volumetric printing conditions and observed under the Zeiss Inverted Microscope (Axiovert 200 M) and Leica Inverted Microscope (DMI6000 B) equipped with cameras (Carl Zeiss AxioCAM MrM, and Hamamatsu C11440) for the characterization of the obtained acoustic patterning.

Data Preprocessing: Solidworks was used to create the CAD models that were used as initial input for the volumetric software. Mario, Pharaoh, Nefertiti bust, liver, lungs, and heart geometries were obtained from Thingiverse.^[84] These files were given to the software in the form of STL. Some of the DiY SonoPrint hardware parts, such as the mechanical fixtures, were designed in Solidworks and sliced using CURA and PreForm software's before 3D printing them with an Ender 3 S1 and Form 3+ printers, respectively.

Calibration Procedure for SonoPrint Printer: Acoustic setups were calibrated using an oscilloscope (Tektronix TBS 2000 series digital oscilloscope 70 MHz 1 GS/s) which is used to measure the resonance frequency of PZT. In addition, for the calibration of the rotational mechanism, high-precision fabrication of the components was employed and was calibrated with a leveler (Emil-Lux Article number: 575 459). It was necessary to design and fabricate a focusing system to ensure the light is focused at the center of the rotational mechanism. This enabled to establish the focusing plane. To calibrate the resin-photo initiator concentration, the absorbency spectrum was calculated on the basis of previous literature.^[65,83]

Post Processing Procedures: Upon completion of printing, isopropanol was used to clean the print. The cleaning was carried out using vibrometer for 10 s repeated five times. After cleaning, the printed structure was placed in vacuum for up to 20 min with UV light. This step was carried to minimize the oxygen inhibition at the structures surface. Later the structure was exposed to UV light for up to 30 min to post-cure the print in UV chamber. Following that, the print was placed in an oven at $85\text{ }^\circ\text{C}$ for 60 min to improve the strength of the printed component. Lastly, the print was again exposed to UV light for up to 20 min.

Pattern Characterization: After printing, the parts were examined under a microscope with cameras. The fabricated geometry was analyzed with SEM (used from facility at BRNC, ETH Zurich). Images taken with microscopes are processed using ImageJ software. For recording the patterning inside the printed geometry, cameras from Blackmagic Design and Canon were used. The tensile test was conducted using a Zwick 1474 testing machine at 1 MPa and a speed of 50 mm min^{-1} , while the compression test utilized a Zwick 1475 testing machine at 20 N and a speed of 10 mm min^{-1} . Both tests were conducted at RMS Foundation, Bettlach, Switzerland. The samples were fabricated in accordance with ASTM D695-23 for compression strength testing, with dimensions of 25.4 mm in height and 12.7 mm in diameter. For tensile testing, samples could not be fabricated with ISO 527-1 norms due to the acoustic setup limitation of printing structures up to 40 mm in height. So, dog bone structures were fabricated with dimensions of 37.5 mm in height, 5.75 mm in width, and 2 mm in depth, half the size specified in ISO 527-1. All samples underwent the same post-processing conditions as those mentioned in post-processing procedures.

Supporting Information

Supporting Information is available from the Wiley Online Library or from the author.

Acknowledgements

Christophe Desarzens, Patrick Colgon, Tomas Garo Gato, and Pascal Graber were acknowledged for their help in optimizing the hardware and software of the SonoPrint printer. The authors thank Zhiyuan Zhang, Mahmoud Medany, and Dimitar Boev for their helpful discussions on acoustic and volumetric setups and Zhan Shi for his help with mechanical simulation for tensile and compression tests. The authors also thank Qiyao Sun, and Erich J. Windhab for the measurement of the viscosity of the resin and Bin Lu and Andreas Stemmer for the measurement of the absorbance spectrum of the resin. The authors thank Designing Alley for their help to create schematics. This project has received funding from the Swiss National Science Foundation (SNSF) under the SNSF Project

funding MINT 2022 grant agreement No 213058, the European Research Council (ERC) under the European Union's Horizon 2020 research and innovation program grant agreement No 853309 (SONOBOTS) and ETH Research Grant, grant agreement No ETH-08 20–1. P.A. acknowledges his funding from BRIDGE under the BRIDGE Proof of Concept Funding 2023 March grant agreement No 218795.

Open access funding provided by Eidgenössische Technische Hochschule Zurich.

Conflict of Interest

The authors declare no conflict of interest.

Author Contributions

D.A. conceived and supervised the project. P.A., S.Z., S.D., and S.M. performed all the experiments with feedback from D.A. P.A. performed the data analysis, designed, and built the system with feedback from D.A. P.A. and D.A. wrote the manuscript. P.A. drew all the figures. All authors contributed to the scientific presentation and discussion and reviewed the manuscript.

Data Availability Statement

The data that support the findings of this study are available in the supplementary material of this article.

Keywords

acoustic, additive manufacturing, composite, SonoPrint, volumetric printing

Received: June 12, 2024
Published online:

- [1] R. N. Yancey, in *Lightweight Composite Structures in Transport* (Ed.: J. Njuguna), Woodhead Publishing, Sawston, UK, **2016**, pp. 35–52.
- [2] J. C. Najmon, S. Raesi, A. Tovar, in *Additive Manufacturing for the Aerospace Industry* (Eds.: F. Froes, R. Boyer), Elsevier, Amsterdam, Netherland, **2019**, pp. 7–31.
- [3] P. D. Mangalgi, *Bull. Mater. Sci.* **1999**, *22*, 657.
- [4] H. Singh, G. Singh Brar, H. Kumar, V. Aggarwal, *Mater. Today Proc.* **2021**, *43*, 320.
- [5] C. E. Bakis, L. C. Bank, V. L. Brown, E. Cosenza, J. F. Davalos, J. J. Lesko, A. Machida, S. H. Rizkalla, T. C. Triantafillou, *J. Compos. Constr.* **2002**, *6*, 73.
- [6] I. Paoletti, *Proc. Eng.* **2017**, *180*, 1150.
- [7] A. Pajonk, A. Prieto, U. Blum, U. Knaack, *J. Build. Eng.* **2022**, *45*, 103603.
- [8] M. S. B. Reddy, D. Ponnamma, R. Choudhary, K. K. Sadasivuni, *Polymers* **2021**, *13*, 1105.
- [9] M. J. Mochane, T. S. Motsoeneng, E. R. Sadiku, T. C. Mokhena, J. S. Sefadi, *Appl. Sci.* **2019**, *9*, 2205.
- [10] C. Richard, A. Neild, V. J. Cadarso, *Lab Chip* **2020**, *20*, 2044.
- [11] A. A. Raheem, P. Hameed, R. Whenish, R. S. Elsen, A. G., A. K. Jaiswal, K. G. Prashanth, G. Manivasagam, *Biomimetics* **2021**, *6*, 65.
- [12] R. Whenish, S. Ramakrishna, A. K. Jaiswal, G. Manivasagam, *Bio-des. Manuf.* **2022**, *5*, 412.
- [13] S. Gervasoni, A. Terzopoulou, C. Franco, A. Veciana, N. Pedrini, J. T. Burri, C. de Marco, E. C. Siringil, X.-Z. Chen, B. J. Nelson, J. Puigmartí-Luis, S. Pané, *Adv. Mater.* **2020**, *32*, 2005652.
- [14] M. Dong, X. Wang, X.-Z. Chen, F. Mushtaq, S. Deng, C. Zhu, H. Torlakcik, A. Terzopoulou, X.-H. Qin, X. Xiao, J. Puigmartí-Luis, H. Choi, A. P. Pêgo, Q.-D. Shen, B. J. Nelson, S. Pané, *Adv. Funct. Mater.* **2020**, *30*, 1910323.
- [15] A. K. Sharma, R. Bhandari, A. Aherwar, R. Rimašauskienė, *Mater. Today Proc.* **2020**, *21*, 1559.
- [16] P. S. Goh, A. F. Ismail, B. C. Ng, *Compos., Part A* **2014**, *56*, 103.
- [17] H. Zhang, L. Zhu, F. Zhang, M. Yang, *Materials* **2021**, *14*, 2223.
- [18] Q. Wang, J. Dai, W. Li, Z. Wei, J. Jiang, *Compos. Sci. Technol.* **2008**, *68*, 1644.
- [19] Y. Yang, X. Li, M. Chu, H. Sun, J. Jin, K. Yu, Q. Wang, Q. Zhou, Y. Chen, *Sci. Adv.* **2019**, *5*, eaau9490.
- [20] D. Kokkinis, M. Schaffner, A. R. Studart, *Nat. Commun.* **2015**, *6*, 8643.
- [21] Y. Ma, Q. Wu, L. Duanmu, S. Wu, Q. Liu, B. Li, X. Zhou, *J. Mater. Sci.* **2020**, *55*, 15510.
- [22] D. S. Melchert, R. R. Collino, T. R. Ray, N. D. Dolinski, L. Friedrich, M. R. Begley, D. S. Gianola, *Adv. Mater. Technol.* **2019**, *4*, 1900586.
- [23] D. E. Yunus, S. Sohrabi, R. He, W. Shi, Y. Liu, *J. Micromech. Microeng.* **2017**, *27*, 045016.
- [24] T. Ma, L. Lv, C. Ouyang, X. Hu, X. Liao, Y. Song, X. Hu, *Carbohydr. Polym.* **2021**, *253*, 117217.
- [25] T. Börzsönyi, B. Szabó, G. Törös, S. Wegner, J. Török, E. Somfai, T. Bien, R. Stannarius, *Phys. Rev. Lett.* **2012**, *108*, 228302.
- [26] A. Sydney Gladman, E. A. Matsumoto, R. G. Nuzzo, L. Mahadevan, J. A. Lewis, *Nat. Mater.* **2016**, *15*, 413.
- [27] S. Choi, K. Y. Lee, S. L. Kim, L. A. MacQueen, H. Chang, J. F. Zimmerman, Q. Jin, M. M. Peters, H. A. M. Ardoña, X. Liu, A.-C. Heiler, R. Gabardi, C. Richardson, W. T. Pu, A. R. Bausch, K. K. Parker, *Nat. Mater.* **2023**, *22*, 1039.
- [28] S. Behr, U. Vainio, M. Müller, A. Schreyer, G. A. Schneider, *Sci. Rep.* **2015**, *5*, 9984.
- [29] R. Sharma, C. Y. Lee, J. H. Choi, K. Chen, M. S. Strano, *Nano Lett.* **2007**, *7*, 2693.
- [30] Y. Wu, R. Chattaraj, Y. Ren, H. Jiang, D. Lee, *Anal. Chem.* **2021**, *93*, 7635.
- [31] T. M. Llewellyn-Jones, B. W. Drinkwater, R. S. Trask, *Smart Mater. Struct.* **2016**, *25*, 02LT01.
- [32] D. Kam, I. Levin, Y. Kutner, O. Lanciano, E. Sharon, O. Shoseyov, S. Magdassi, *Polymers* **2022**, *14*, 733.
- [33] S. Safaee, M. Schock, E. B. Joyee, Y. Pan, R. K. Chen, *Addit. Manuf.* **2022**, *51*, 102642.
- [34] Z. Zhang, A. Sukhov, J. Harting, P. Margaretti, D. Ahmed, *Nat. Commun.* **2022**, *13*, 7347.
- [35] J. Madrid-Wolff, A. Boniface, D. Loterie, P. Delrot, C. Moser, *Adv. Sci.* **2022**, *9*, 2105144.
- [36] P. S. Kollipara, Z. Chen, Y. Zheng, *ACS Nano* **2023**, *17*, 7051.
- [37] P. S. Kollipara, X. Li, J. Li, Z. Chen, H. Ding, Y. Kim, S. Huang, Z. Qin, Y. Zheng, *Nat. Commun.* **2023**, *14*, 5133.
- [38] Z. Shi, D. Pu, R. Huan, X. Wang, Z. Jiang, X. Wei, *Mech. Syst. Signal Process.* **2022**, *177*, 109164.
- [39] A. J. Pascall, F. Qian, G. Wang, M. A. Worsley, Y. Li, J. D. Kuntz, *Adv. Mater.* **2014**, *26*, 2252.
- [40] I. Liaschenko, J. Rosell-Llompарт, A. Cabot, *Nat. Commun.* **2020**, *11*, 753.
- [41] M. Kunitski, N. Eicke, P. Huber, J. Köhler, S. Zeller, J. Voigtsberger, N. Schlott, K. Henrichs, H. Sann, F. Trinter, L. P. H. Schmidt, A. Kalinin, M. S. Schöffler, T. Jahnke, M. Lein, R. Dörner, *Nat. Commun.* **2019**, *10*, 1.
- [42] P. Romano, H. Fabritius, D. Raabe, *Acta Biomater.* **2007**, *3*, 301.
- [43] J. Li, X. Liang, F. Liou, J. Park, *Sci. Rep.* **2018**, *8*, 1846.
- [44] Y. Yang, Z. Chen, X. Song, Z. Zhang, J. Zhang, K. K. Shung, Q. Zhou, Y. Chen, *Adv. Mater.* **2017**, *29*, 1605750.
- [45] D. Han, C. Yang, N. X. Fang, H. Lee, *Addit. Manuf.* **2019**, *27*, 606.

- [46] J. J. Martin, B. E. Fiore, R. M. Erb, *Nat. Commun.* **2015**, *6*, 8641.
- [47] R. M. Erb, D. S. Sebba, A. A. Lazarides, B. B. Yellen, *J. Appl. Phys.* **2008**, *103*, 063916.
- [48] X. Wang, M. Jiang, Z. Zhou, J. Gou, D. Hui, *Composites, Part B* **2017**, *110*, 442.
- [49] H. Song, J. Spencer, A. Jander, J. Nielsen, J. Stasiak, V. Kasperchik, P. Dhagat, *J. Appl. Phys.* **2014**, *115*, 17E308.
- [50] T. Nakamoto, S. Kojima, *J. Adv. Mech. Des. Syst., Manuf.* **2012**, *6*, 849.
- [51] W. C. Liu, V. H. Y. Chou, R. P. Behera, H. L. Ferrand, *Nat. Commun.* **2022**, *13*, 5015.
- [52] Y. Wang, C. Xu, J. Liu, H. Pan, Y. Li, D. Mei, *Addit. Manuf.* **2022**, *60*, 103247.
- [53] J. Durrer, P. Agrawal, A. Ozgul, S. C. F. Neuhaus, N. Nama, D. Ahmed, *Nat. Commun.* **2022**, *13*, 6370.
- [54] K. Johnson, D. Melchert, D. S. Gianola, M. Begley, T. R. Ray, *MRS Adv.* **2021**, *6*, 636.
- [55] P. Agrawal, Z. Zhang, Z. Ghorbanikharaji, Z. Shi, D. Ahmed, in *Robotics for Cell Manipulation and Characterization* (Eds.: C. Dai, G. Shan, Y. Sun), Academic Press, Cambridge, MA, US, **2023**, pp. 329–353.
- [56] A. Del Campo Fonseca, C. Glück, J. Droux, Y. Ferry, C. Frei, S. Wegener, B. Weber, M. El Amki, D. Ahmed, *Nat. Commun.* **2023**, *14*, 5889.
- [57] V. M. Jooss, J. S. Bolten, J. Huwyler, D. Ahmed, *Sci. Adv.* **2022**, *8*, eabm2785.
- [58] C. Dillinger, N. Nama, D. Ahmed, *Nat. Commun.* **2021**, *12*, 6455.
- [59] Y. Deng, A. Paskert, Z. Zhang, R. Wittkowski, D. Ahmed, *Sci. Adv.* **2023**, *9*, eadh5260.
- [60] C. Richard, C. Devendran, D. Ashtiani, V. J. Cadarso, A. Neild, *Lab Chip* **2022**, *22*, 3533.
- [61] L. Lu, X. Tang, S. Hu, Y. Pan, *3D Print. Addit. Manuf.* **2018**, *5*, 151.
- [62] M.-S. Scholz, B. W. Drinkwater, R. S. Trask, *Ultrasonics* **2014**, *54*, 1015.
- [63] K. Niendorf, B. Raeymaekers, *Comput. Mater. Sci.* **2022**, *206*, 111233.
- [64] X. Li, K. M. Lim, W. Zhai, *Appl. Mater. Today* **2022**, *26*, 101388.
- [65] B. E. Kelly, I. Bhattacharya, H. Heidari, M. Shusteff, C. M. Spadaccini, H. K. Taylor, *Science* **2019**, *363*, 1075.
- [66] P. N. Bernal, P. Delrot, D. Loterie, Y. Li, J. Malda, C. Moser, R. Levato, *Adv. Mater.* **2019**, *31*, 1904209.
- [67] A. A. Doinikov, *J. Fluid Mech.* **1994**, *267*, 1.
- [68] Z. Meng, X. Zhai, J. Wei, Z. Wang, H. Wu, *Sensors* **2018**, *18*, 1143.
- [69] D. Ahmed, A. Sukhov, D. Hauri, D. Rodrigue, G. Maranta, J. Harting, B. J. Nelson, *Nat. Mach. Intell.* **2021**, *3*, 116.
- [70] H. Bruus, *Lab Chip* **2012**, *12*, 1014.
- [71] M. Settnes, H. Bruus, *Phys. Rev. E* **2012**, *85*, 016327.
- [72] M. Barmatz, P. Collas, *J. Acoust. Soc. Am.* **1985**, *77*, 928.
- [73] H. Bruus, *Lab Chip* **2012**, *12*, 1014.
- [74] M. Xie, L. Lian, X. Mu, Z. Luo, C. E. Garciamendez-Mijares, Z. Zhang, A. López, J. Manríquez, X. Kuang, J. Wu, J. K. Sahoo, F. Z. González, G. Li, G. Tang, S. Maharjan, J. Guo, D. L. Kaplan, Y. S. Zhang, *Nat. Commun.* **2023**, *14*, 210.
- [75] C. E. Garciamendez-Mijares, P. Agrawal, G. García Martínez, E. Cervantes Juarez, Y. S. Zhang, *Appl. Phys. Rev.* **2021**, *8*, 031312.
- [76] M. Aliabouzar, A. W. Y. Ley, S. Meurs, A. J. Putnam, B. M. Baker, O. D. Kripfgans, J. B. Fowlkes, M. L. Fabiilli, *Int. J. Bioprint.* **2022**, *25*, e00188.
- [77] Y. Sriphutkiat, S. Kasetsirikul, D. Ketpun, Y. Zhou, *Sci. Rep.* **2019**, *9*, 17774.
- [78] R. R. Collino, T. R. Ray, R. C. Fleming, J. D. Cornell, B. G. Compton, M. R. Begley, *Extreme Mech. Lett.* **2016**, *8*, 96.
- [79] R. R. Collino, T. R. Ray, L. M. Friedrich, J. D. Cornell, C. D. Meinhart, M. R. Begley, *Mater. Res. Lett.* **2018**, *6*, 191.
- [80] J. Wang, F. Soto, P. Ma, R. Ahmed, H. Yang, S. Chen, J. Wang, C. Liu, D. Akin, K. Fu, X. Cao, P. Chen, E.-C. Hsu, H. T. Soh, T. Stoyanova, J. C. Wu, U. Demirci, *ACS Nano* **2022**, *16*, 10219.
- [81] J. P. K. Armstrong, J. L. Puetzer, A. Serio, A. G. Guex, M. Kapnisi, A. Breant, Y. Zong, V. Assal, S. C. Skaalure, O. King, T. Murty, C. Meinert, A. C. Franklin, P. G. Bassindale, M. K. Nichols, C. M. Terracciano, D. W. Hutmacher, B. W. Drinkwater, T. J. Klein, A. W. Perriman, M. M. Stevens, *Adv. Mater.* **2018**, *30*, 1802649.
- [82] J. Madrid-Wolff, J. Toombs, R. Rizzo, P. N. Bernal, D. Porcincula, R. Walton, B. Wang, F. Kotz-Helmer, Y. Yang, D. Kaplan, Y. S. Zhang, M. Zenobi-Wong, R. R. McLeod, B. Rapp, J. Schwartz, M. Shusteff, H. Talyor, R. Levato, C. Moser, *MRS Commun.* **2023**, *13*, 764.
- [83] D. Loterie, P. Delrot, C. Moser, *Nat. Commun.* **2020**, *11*, 852.
- [84] Thingiverse.com, “Thingiverse – Digital Designs for Physical Objects”, <https://www.thingiverse.com> (accessed: May 2024).